Redox-Active Cavitands

DOI: 10.1002/anie.201106031

Quinone-Based, Redox-Active Resorcin[4]arene Cavitands**

*Igor Pochorovski, Corinne Boudon, Jean-Paul Gisselbrecht, Marc-Olivier Ebert, W. Bernd Schweizer, and François Diederich**

Since the preparation of the first quinoxaline-bridged resorcin[4]arene cavitand by Cram and co-workers in 1982,[1] numerous derivatives with various structures and functions have been prepared and employed as switches,[2] receptors and sensors,[3] catalysts,[4] and molecular hosts.[5] The most fascinating feature of top-open resorcin[4]arene cavitands is their ability to adopt two spatially well-defined conformations: an expanded "kite" form and a contracted "vase" form. While various methods have been employed to study the conformational properties of cavitands,[6] the most convenient one is ^{1}H NMR spectroscopy. Figure 1 illustrates the vase–kite1–kite2 equilibrium of a generic cavitand, and how three situations, vase, kite with slow kite1–kite2 interconversion, and kite with fast kite1–kite2 interconversion, can be distinguished by ^{1}H NMR spectroscopy.[7]

The three stimuli that have been identified for switching the cavitand between its vase and kite forms are changes in temperature,[1,8] pH,[9] and metal-ion concentration.[6a] Additionally, cavitands can function as molecular grippers by binding guest molecules in their vase conformations; these binding properties have been modulated using changes in pH,[10] metal-ion complexation,[11] and light.[12] To use redox processes as new stimuli for tuning cavitand properties, however, is a highly desirable, yet unreached goal.[2] Electrochemically induced redox switching, if truly reversible, and performed on the surface of a metal electrode, could enable the application of cavitands as molecular grippers.[2,13] Towards this end, we chose to investigate cavitands containing the quinone moiety as a new and easily installed redox-active wall component[8b] and to study how changing their redox states affects their conformational and binding properties.

It has been shown that cavitand wall size and solvent identity can influence the vase–kite equilibrium of resorcin[4]arene cavitands:[6e,7,14] the vase conformation is preferred more strongly in cavitands with larger walls and in solvents such as tetrahydrofuran, benzene, and toluene than in cavitands with smaller walls and in chlorinated solvents (CD_2Cl_2, $CDCl_3$, $(CDCl_2)_2$). We therefore prepared a series of quinoid cavitands with different wall sizes (ox-**1a**–**c**, Figure 2) and investigated their conformational preferences in one member of each solvent class (for the synthesis of all reported compounds, see the Supporting Information, Section 2).

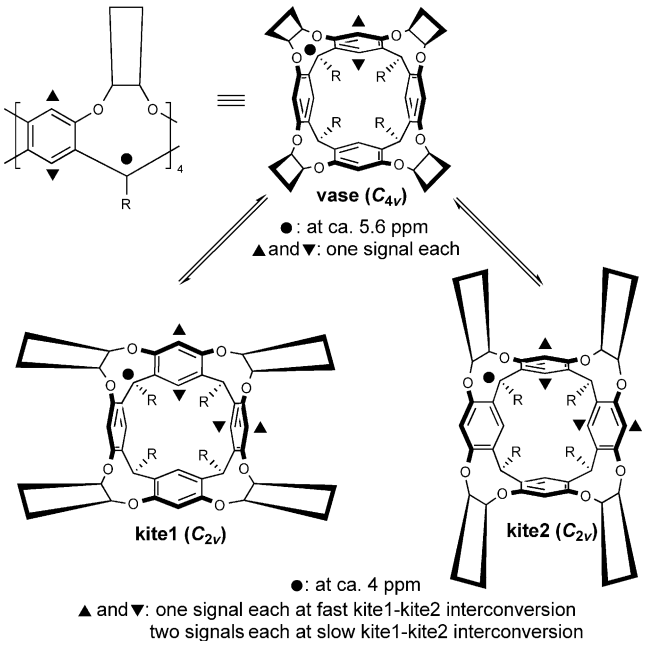

Figure 1. Vase–kite1–kite2 equilibrium of a generic cavitand and summary of characteristic ^{1}H NMR features of three situations: vase, kite with slow kite1–kite2 interconversion, and kite with fast kite1–kite2 interconversion.

The ^{1}H NMR spectra (298 K, 500 MHz) of cavitand ox-**1b** in CD_2Cl_2 and [D_8]THF are shown in Figure 2. In both solvents, the cavitand is present in the kite conformation: the methine protons (●) are located at 4.25 ppm in CD_2Cl_2 and at 4.43 ppm in [D_8]THF, respectively. The main difference between the two solvents, however, is that in CD_2Cl_2, two sharp signals are observed for each of the bowl protons (▲ and ▼), while in [D_8]THF, these signals are close to coalescence. This indicates that the kite1–kite2 interconversion is faster in [D_8]THF than in CD_2Cl_2. Thus, [D_8]THF not only stabilizes the vase conformation more strongly but also the vaselike transition state[7] for the kite1–kite2 interconversion. The preference of cavitand ox-**1b** for the kite conformation was

[*] I. Pochorovski, Dr. M.-O. Ebert, Dr. W. B. Schweizer, Prof. Dr. F. Diederich
Laboratorium für Organische Chemie, ETH Zürich
Hönggerberg, HCI, 8093 Zürich (Switzerland)
E-mail: diederich@org.chem.ethz.ch
Prof. Dr. C. Boudon, Dr. J.-P. Gisselbrecht
Laboratoire d'Electrochimie et de Chimie Physique du Corps Solide
Institut de Chimie-UMR 7177, C.N.R.S., Université de Strasbourg
4, rue Blaise Pascal, 67081 Strasbourg Cedex (France)

[**] This work was supported by a grant from the Swiss National Science Foundation (SNF). I.P. acknowledges the receipt of a fellowship from the Fonds der Chemischen Industrie. We thank Prof. Dr. Bernhard Jaun for helpful discussions and Dr. Melanie Chiu for reviewing the manuscript.

Supporting information for this article is available on the WWW under http://dx.doi.org/10.1002/anie.201106031.

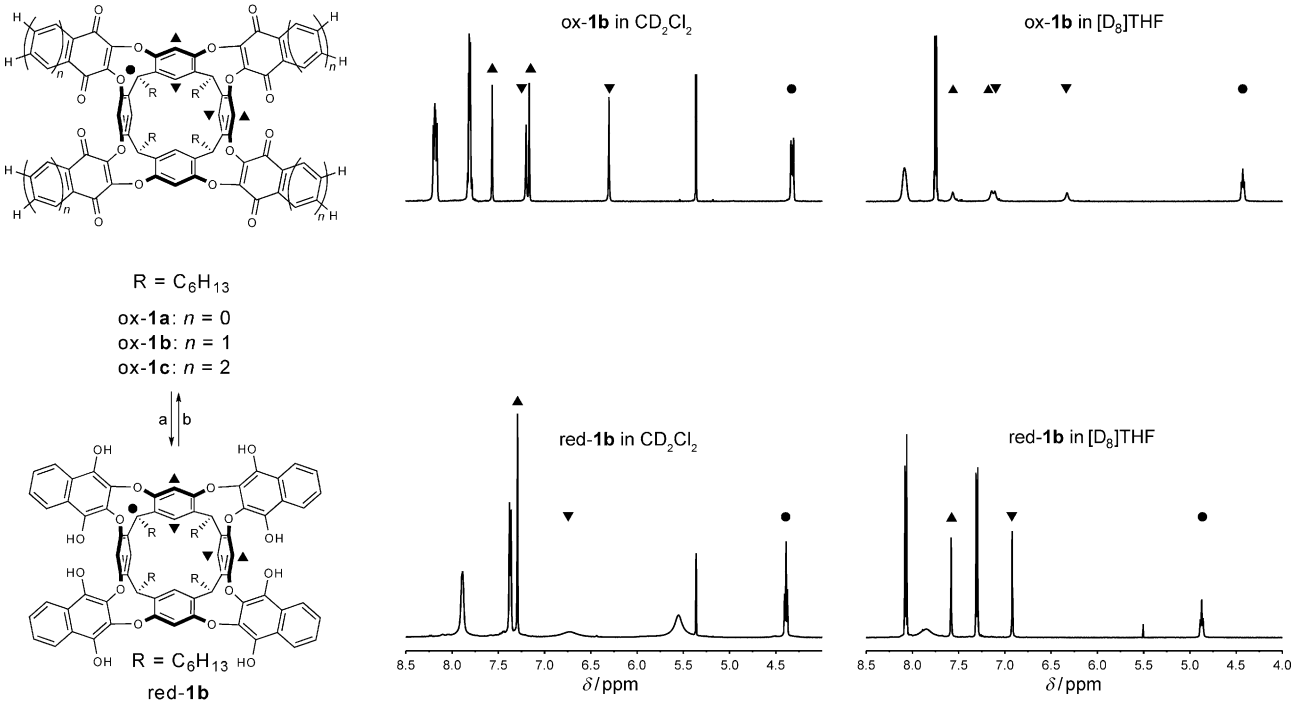

Figure 2. Left: Cavitands ox-**1a–c** and redox interconversion between the quinone and hydroquinone states of cavitand **1b**. a) $Na_2S_2O_4$, $CDCl_3/H_2O$ (degassed), 60 °C, 3 h, quantitative. b) Air, quantitative. Sections of the ^{1}H NMR spectra (298 K, 500 MHz) of cavitands ox-**1b** and red-**1b** in CD_2Cl_2 (middle) and [D_8]THF (right).

further supported by its X-ray crystal structure (crystals from acetone), which shows the cavitand in the kite form (Figure 3, upper left; for details on X-ray analyses, see Section 4 in the Supporting Information).

The activation parameters for the kite1–kite2 interconversion of ox-**1a–c** in CD_2Cl_2 and [D_8]THF are presented in Table 1.[15] These data show that in general, increasing wall size (e.g. ox-**1a** to ox-**1c**) leads to a slight decrease in $\Delta G^{\ddagger}_{298\,K}$, which correlates with an increased ^{1}H NMR chemical shift of the methine protons. However, the influence of wall size on $\Delta G^{\ddagger}_{298\,K}$ is small compared to the influence of the solvent: $\Delta G^{\ddagger}_{298\,K}$ in [D_8]THF is, on average, about 0.8 kcal mol^{-1} lower than in CD_2Cl_2 for each cavitand.

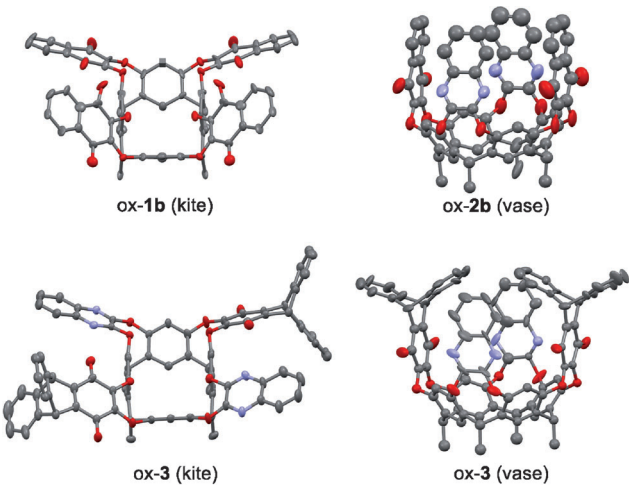

Figure 3. Crystal structures of cavitands ox-**1b** (top left, from acetone), ox-**2b** (top right, from DMF), ox-**3** (bottom left, from [D_{12}]mesitylene), and ox-**3** (bottom right, from DMF) at 100 K. Solvent molecules, *n*-hexyl chains, and hydrogen atoms are omitted for clarity. Thermal ellipsoids are shown at the 50% probability level.

For chemical redox-switching studies on the tetraquinone-cavitand class, we selected the medium-sized cavitand ox-**1b**, which was chemically reduced to the corresponding hydroquinone form, red-**1b**, with $Na_2S_2O_4$ (Figure 2). Cavitand red-**1b** cleanly reverts to ox-**1b** upon exposure to air. This redox reversibility was confirmed by cyclic voltammetry (CV) and rotating-disk voltammetry (RDV).[16] The ^{1}H NMR spectra (298 K, 500 MHz) of cavitand red-**1b** in CD_2Cl_2 and [D_8]THF shown in Figure 2 indicate the presence of the kite form in both solvents.[17] However, the methine proton signals in red-**1b** are shifted downfield compared to the methine protons of ox-**1b**, and the aromatic protons (▲ and ▼) exhibit only one signal each. Thus, in both solvents, the vaselike transition state for the kite1–kite2 interconversion is stabilized upon reduction of the cavitand from the quinone to the hydroquinone state. However, this stabilization is not sufficient to fully switch the cavitand into the vase form, the prevalence of which is a prerequisite for binding.

We presumed that in ox-**1a–c**, C=O···C=O repulsions between neighboring walls prohibit access to the vase conformation. In order to reduce these repulsive interactions, we prepared the diquinone-cavitand series ox-**2a–c** (Figure 4). A minor influence of wall size on cavitand conformation was also observed for this series. Figure 4 shows ^{1}H NMR spectra (298 K, 300 MHz) of cavitand ox-**2b** in CD_2Cl_2 and [D_8]THF. In CD_2Cl_2, ox-**2b** is present in the

Table 1: Kinetic parameters ($\Delta H^{\neq}$, $\Delta S^{\neq}$, and $\Delta G^{\neq}_{298\,K}$) for the kite1–kite2 interconversion, thermodynamic quantities (ΔH, ΔS, and $\Delta G_{298\,K}$) for the vase→kite equilibrium, and chemical shifts $\delta_{298\,K}$ (●) of the methine protons of cavitands ox-**1a–c**, red-**1b**, ox-**2b**, and red-**2b**, in various solvents.[a]

Cavitand	Solvent	Process	$\Delta H^{\neq}$ [kcal mol^{-1}]	$\Delta S^{\neq}$ [cal mol^{-1} K^{-1}]	$\Delta G^{\neq}_{298\,K}$ [kcal mol^{-1}]	ΔH [kcal mol^{-1}]	ΔS [cal mol^{-1} K^{-1}]	$\Delta G_{298\,K}$ [kcal mol^{-1}]	$\delta_{298\,K}$ (●)[ppm]
ox-**1a**	$(CDCl_2)_2$	kite1→kite2	15.8±0.3	−2.5±1.1	16.6±0.5	–	–	–	4.15
ox-**1b**	$(CDCl_2)_2$	kite1→kite2	17.2±0.3	4.2±1.2	16.0±0.5	–	–	–	4.25
ox-**1c**	$(CDCl_2)_2$	kite1→kite2	16.6±0.4	2.0±1.3	16.0±0.5	–	–	–	4.30
ox-**1a**	[D$_8$]THF	kite1→kite2	13.7±0.4	−6.4±1.5	15.7±0.6	–	–	–	4.35
ox-**1b**	[D$_8$]THF	kite1→kite2	14.4±0.2	−2.9±0.8	15.3±0.3	–	–	–	4.43
ox-**1c**	[D$_8$]THF	kite1→kite2	n.d.	n.d.	n.d.	–	–	–	4.51
red-**1b**	$(CDCl_2)_2$	kite1→kite2	n.b.	n.d.	n.d.	–	–	–	4.39
red-**1b**	[D$_8$]THF	kite1→kite2	7.7±0.4[b]	−8.4±1.6[b]	10.2±0.6[b]	–	–	–	4.87
ox-**2b**	CD_2Cl_2	kite1→kite2	15.6±0.2	9.5±0.6	12.8±0.3	–	–	–	4.36, 3.74
ox-**2b**	[D$_8$]THF	vase→kite	–	–	–	−3.0±0.1	−16.1±0.5	1.8±0.2	5.59 br
red-**2b**	CD_2Cl_2	kite1→kite2	n.d.	n.d.	n.d.	–	–	–	4.48, 3.53
red-**2b**	[D$_8$]THF	vase→kite	–	–	–	−0.7±0.1	−6.8±0.6	1.3±0.2	5.79, 5.62

[a] $\Delta H^{\neq}$, $\Delta S^{\neq}$, and $\Delta G^{\neq}_{298\,K}$ determined using inversion-transfer NMR experiments at various temperatures and subsequent Eyring analysis, unless otherwise stated. ΔH, ΔS, and $\Delta G_{298\,K}$ determined by integration of distinct ^{1}H NMR signals corresponding to the vase and kite conformations at low temperatures and subsequent van't Hoff analysis. Errors are given at the 95% confidence level. n.d. = not determined because of poor solubility. [b] Determined using iterative line-shape fitting of variable-temperature ^{1}H NMR spectra and subsequent Eyring analysis.

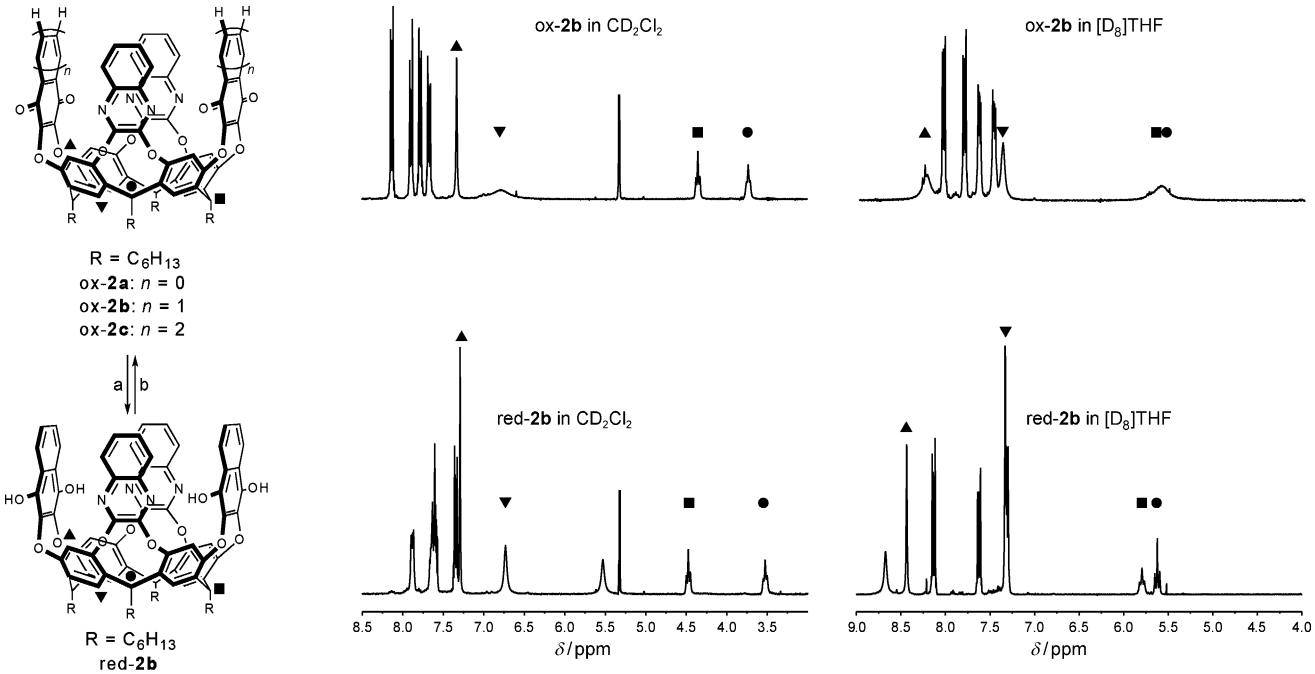

Figure 4. Left: Cavitands ox-**2a–c** and redox interconversion between the quinone and hydroquinone states of cavitand **2b**. a) $Na_2S_2O_4$, $CDCl_3/H_2O$ (degassed), 60 °C, 3 h, quantitative. b) Air, quantitative. Sections of the ^{1}H NMR spectra (298 K, 300 MHz) of cavitands ox-**2b** and red-**2b** in CD_2Cl_2 (middle) and [D$_8$]THF (right).

kite conformation,[18] though the activation barrier for the kite1–kite2 interconversion is significantly lower (12.8 kcal mol^{-1}) than that of ox-**1b** (16.0 kcal mol^{-1}). In contrast, [D$_8$]THF provides the requisite stabilization for ox-**2b** to access the vase conformation: the methine protons appear at 5.59 ppm as a broad signal. X-ray crystallographic studies further support the higher intrinsic preference of cavitand ox-**2b** for the vase conformation; it crystallized in the vase form from DMF (Figure 3, upper right).[19] ^{1}H NMR spectra (298 K, 300 MHz) of red-**2b**, the reduced form of ox-**2b**, in CD_2Cl_2 and [D$_8$]THF are shown in Figure 4. The conformational preferences do not significantly change: as with ox-**2b**, red-**2b** is present in the kite form in CD_2Cl_2 and in the vase form in [D$_8$]THF.

Having investigated the conformational and electrochemical properties of the new cavitands, we turned our attention to binding studies. These were performed in [D$_{12}$]mesitylene, which is too big to be able to compete with guests for the binding site. Similar to other open-top cavitands, however, binding of various aromatic and alicyclic molecules was weak ($K_a < 2$), with fast guest exchange on the NMR timescale.[20] We attributed this to the open-top structure of the cavi-

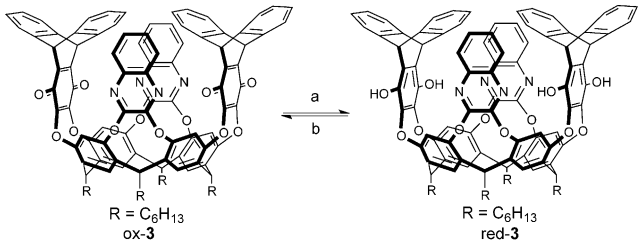

Figure 5. Redox interconversion between the quinone and hydroquinone states of cavitand **3**. a) H_2, Pd/C, THF (degassed), 25 °C, 30 min, quantitative. b) Air, quantitative.

tands[6e,10] and to their structural flexibility.[21] To address the first issue, we prepared the triptycene-derived diquinone cavitand ox-**3** and its reduced form, red-**3** (Figure 5).

^{1}H NMR studies showed that the conformational properties of cavitands ox-**3** and red-**3** are very similar to those of cavitands ox-**2a–c** and red-**2a–c**. However, ox-**3** and red-**3** form kinetically stable host–guest complexes on the NMR timescale with various cycloalkanes, with the highest binding constants measured for cyclohexane (Table 2). In pure

Table 2: Association constants K_a between cavitands ox-**3** and red-**3**, and various cycloalkanes ([D_{12}]mesitylene, 298 K).[a,b]

Guest	K_a(ox-**3**⊂guest) [M^{-1}]	K_a(red-**3**⊂guest) [M^{-1}]
cyclopentane	3.2	< 0.1
cyclohexane	19.2	3.1
cycloheptane	6.3	1.6

[a] Determined by integration of the ^{1}H NMR resonances of the relevant species, relative to 1,3,5-trimethoxybenzene as an internal standard. [b] Error in K_a is estimated to be roughly 20%.

[D_{12}]mesitylene, ox-**3** and red-**3** are present in the kite conformation (the methine protons appear at 3.9 and 4.1 ppm (ox-**3**) and at 3.9 and 4.5 ppm (red-**3**); see Section 6 in the Supporting Information). Upon addition of excess cyclohexane, guest-induced switching to the vase conformation occurs in both ox-**3** and red-**3** (the methine protons shift to 5.8 and 5.9 ppm (ox-**3** complex) and to 5.9 and 6.0 ppm (red-**3** complex)), and encapsulated cyclohexane is observed (−2.9 ppm (ox-**3** complex) and −3.2 (red-**3** complex)). Importantly, the K_a values of complexes of cavitand ox-**3** are higher than those of red-**3** (Table 2). This is possibly because $\Delta G_{298\,K}$ for the kite→vase switching of ox-**3** is smaller than that of red-**3**, in analogy to the difference in the kite→vase switching processes of the ox-**2b**/red-**2b** pair (Table 1). Complete guest release was showcased for ox-**3**: protonation of the quinoxaline nitrogens using trifluoroacetic acid (TFA) switched the cavitand back to the kite conformation, thereby releasing cyclohexane.

X-ray crystal structures showing cavitand ox-**3** in both conformations, vase and kite, were obtained (Figure 3): ox-**3** crystallized in the vase form from DMF and in the kite form from [D_{12}]mesitylene, which also reflects the solution-state conformational preferences of ox-**3** in these solvents. ox-**3** is the first resorcin[4]arene-based cavitand that has been crystallized in both the vase and kite forms, highlighting the fact that cavitands of this type have no inherent preference for one conformation over the other, such that mainly solvent influence determines the observed conformation.

In summary, we have prepared and studied novel, redox-active, quinone-based resorcin[4]arene cavitands. Cavitands with four quinone units exist only in the kite conformation, while cavitands containing two quinone and two quinoxaline units can access both the kite and the vase forms. Their actual, observed conformation is strongly solvent dependent. For the first time, X-ray structures of both the vase and kite forms of a resorcin[4]arene-based cavitand (ox-**3**) were obtained. The top-covered cavitands ox/red-**3** form kinetically stable host–guest complexes on the NMR timescale with various cycloalkanes. Guest release can be induced by protonation of the quinoxaline nitrogens. Notably, the binding strength can also be modulated by changing the redox state of the cavitand. Now that we have demonstrated the proof of principle for the redox switching of cavitand properties, developing cavitands in which the redox-switching is even more pronounced would bring us closer to utilizing cavitands in advanced-materials applications.

Received: August 26, 2011
Published online: November 14, 2011

Keywords: cavitands · host–guest systems · quinones · redox switching · supramolecular chemistry

[1] J. R. Moran, S. Karbach, D. J. Cram, *J. Am. Chem. Soc.* **1982**, *104*, 5826–5828.
[2] V. A. Azov, A. Beeby, M. Cacciarini, A. G. Cheetham, F. Diederich, M. Frei, J. K. Gimzewski, V. Gramlich, B. Hecht, B. Jaun, T. Latychevskaia, A. Lieb, Y. Lill, F. Marotti, A. Schlegel, R. R. Schlittler, P. J. Skinner, P. Seiler, Y. Yamakoshi, *Adv. Funct. Mater.* **2006**, *16*, 147–156.
[3] a) M. Melegari, M. Suman, L. Pirondini, D. Moiani, C. Massera, F. Ugozzoli, E. Kalenius, P. Vainiotalo, J. C. Mulatier, J. P. Dutasta, E. Dalcanale, *Chem. Eur. J.* **2008**, *14*, 5772–5779; b) L. Pirondini, E. Dalcanale, *Chem. Soc. Rev.* **2007**, *36*, 695–706.
[4] a) B. W. Purse, J. Rebek, *Proc. Natl. Acad. Sci. USA* **2005**, *102*, 10777–10782; b) R. J. Hooley, J. Rebek, *Chem. Biol.* **2009**, *16*, 255–264.
[5] a) J. Rebek, *Acc. Chem. Res.* **2009**, *42*, 1660–1668; b) F. Hof, S. L. Craig, C. Nuckolls, J. Rebek, *Angew. Chem.* **2002**, *114*, 1556–1578; *Angew. Chem. Int. Ed.* **2002**, *41*, 1488–1508.
[6] a) M. Frei, F. Marotti, F. Diederich, *Chem. Commun.* **2004**, 1362–1363; b) P. Pagliusi, F. Lagugne-Labarthet, D. K. Shenoy, E. Dalcanale, Y. R. Shen, *J. Am. Chem. Soc.* **2006**, *128*, 12610–12611; c) V. A. Azov, A. Schlegel, F. Diederich, *Angew. Chem.* **2005**, *117*, 4711–4715; *Angew. Chem. Int. Ed.* **2005**, *44*, 4635–4638; d) I. Pochorovski, B. Breiten, W. B. Schweizer, F. Diederich, *Chem. Eur. J.* **2010**, *16*, 12590–12602; e) L. D. Shirtcliff, H. Xu, F. Diederich, *Eur. J. Org. Chem.* **2010**, 846–855.
[7] V. A. Azov, B. Jaun, F. Diederich, *Helv. Chim. Acta* **2004**, *87*, 449–462.
[8] a) J. R. Moran, J. L. Ericson, E. Dalcanale, J. A. Bryant, C. B. Knobler, D. J. Cram, *J. Am. Chem. Soc.* **1991**, *113*, 5707–5714; b) D. J. Cram, L. M. Tunstad, C. B. Knobler, *J. Org. Chem.* **1992**, *57*, 528.
[9] P. J. Skinner, A. G. Cheetham, A. Beeby, V. Gramlich, F. Diederich, *Helv. Chim. Acta* **2001**, *84*, 2146–2153.

[10] a) T. Gottschalk, B. Jaun, F. Diederich, *Angew. Chem.* **2007**, *119*, 264 – 268; *Angew. Chem. Int. Ed.* **2007**, *46*, 260 – 264; b) T. Gottschalk, P. D. Jarowski, F. Diederich, *Tetrahedron* **2008**, *64*, 8307 – 8317.
[11] F. Durola, J. Rebek, *Angew. Chem.* **2010**, *122*, 3257 – 3259; *Angew. Chem. Int. Ed.* **2010**, *49*, 3189 – 3191.
[12] O. B. Berryman, A. C. Sather, J. Rebek, *Chem. Commun.* **2011**, *47*, 656 – 658.
[13] M. Frei, F. Diederich, R. Tremont, T. Rodriguez, L. Echegoyen, *Helv. Chim. Acta* **2006**, *89*, 2040 – 2057.
[14] P. Roncucci, L. Pirondini, G. Paderni, C. Massera, E. Dalcanale, V. A. Azov, F. Diederich, *Chem. Eur. J.* **2006**, *12*, 4775 – 4784.
[15] A detailed description about how activation parameters have been determined is given in the the Supporting Information (Section 5).
[16] Detailed information on the CV and RDV data of all new compounds and substituted quinone and quinoxaline reference compounds are in the Supporting Information (Section 7).
[17] A variable-temperature (VT) NMR scan in [D_8]THF showed that upon cooling, the methine protons of red-**1b** decoalesce and reappear as two broad signals at 5.9 ppm and 4.7 ppm below 210 K (see Section 5.6 in the Supporting Information). Such VT behavior has not been observed for resorcin[4]arene cavitands. Two different dynamic processes could account for the observed low-temperature spectrum: 1) a slow vase–kite interconversion; 2) a slow interconversion between structures in which two walls are in the kite position and two in the vase. VT NMR analysis of red-**1b** in CD_2Cl_2 was hampered by gelation at low temperatures.
[18] Two sets of methine protons located at 3.74 ppm and 4.36 ppm are observed. In analogy to tetraquinone- and tetraquinoxaline-cavitands, the signal at 3.74 ppm can be assigned to the methine protons below the quinoxaline unit, while the signal at 4.36 ppm corresponds to methine protons below the quinone wall.
[19] An X-ray structure (crystals obtained from toluene) also showing cavitand ox-**2b** in the vase conformation is in the Supporting Information (Section 4.4).
[20] For more details on these binding experiments see the Supporting Information (Section 8).
[21] D. M. Rudkevich, G. Hilmersson, J. Rebek, *J. Am. Chem. Soc.* **1998**, *120*, 12216 – 12225.

